Volume 13
Number 47
21 December 2025
Pages 23283–23662

Journal of Materials Chemistry C

Materials for optical, magnetic and electronic devices

rsc.li/materials-c

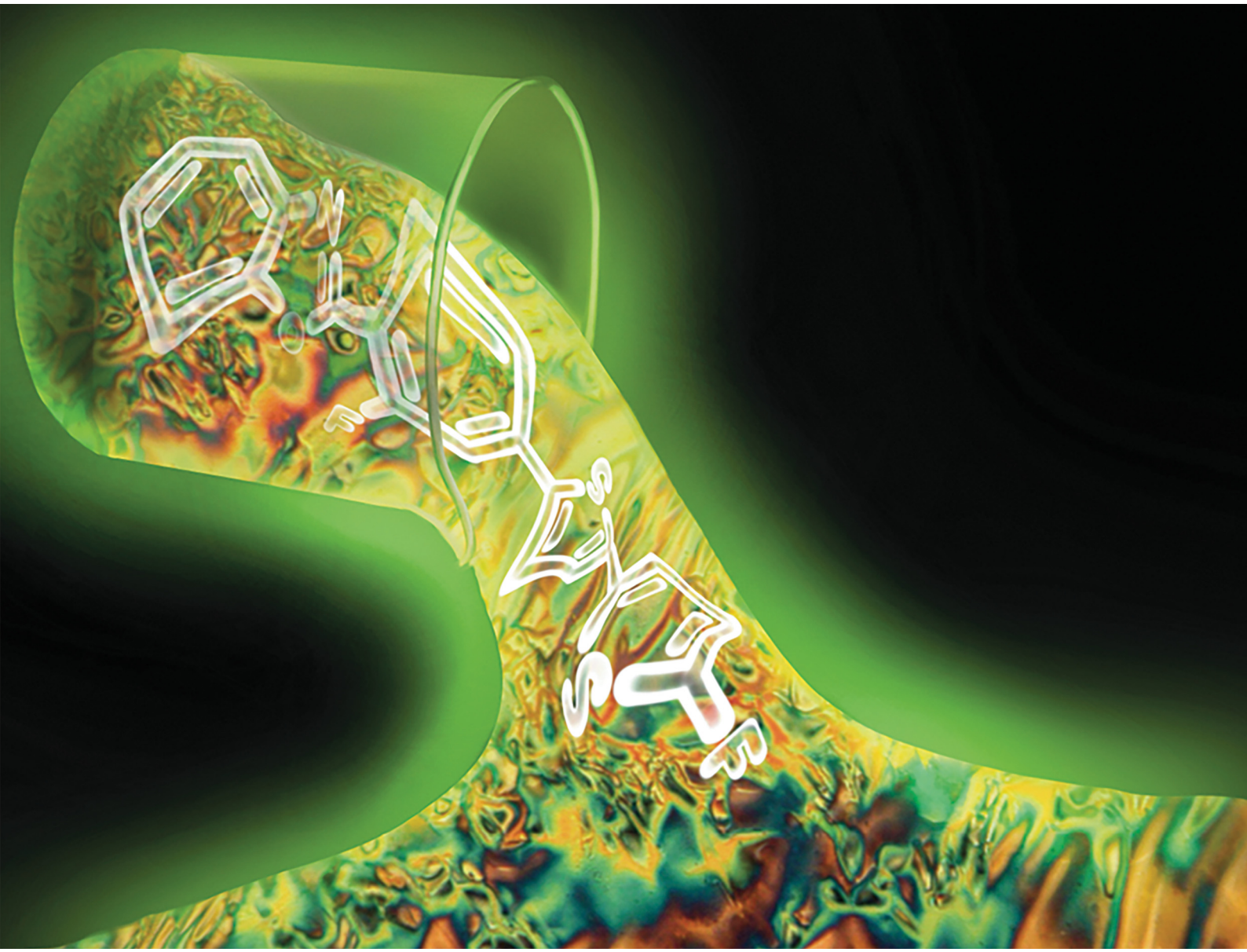

ISSN 2050-7526

ROYAL SOCIETY OF CHEMISTRY

PAPER

S. Holger Eichhorn *et al.*

Fluorination in core-only calamitic liquid crystals: how many and where should they go?

Journal of Materials Chemistry C

ROYAL SOCIETY OF CHEMISTRY

PAPER

View Article Online
View Journal | View Issue

Cite this: J. Mater. Chem. C, 2025, 13, 23379

Fluorination in core-only calamitic liquid crystals: how many and where should they go?

Jacob G. Rothera,[a] Reem Bazzi,[a] Lara K. Watanabe,[a] Jeremy M. Rawson,[a] A. Mohan Raj,[b] William G. Skene[b] and S. Holger Eichhorn*[a]

Introducing fluorine as a lateral substituent within the conjugated cores of conventional, side-chain bearing calamitic liquid crystals has been shown to provide either enhanced or detrimental effects on mesomorphic properties depending on the number and substitution location of the fluorine atom(s) within the mesogenic core. The slightly larger size of fluorine compared to hydrogen combined with its vastly differing electronic properties serve to control molecular packing during mesophase formation that can contribute to stabilizing or selecting for a certain mesophase type, induce new, higher ordered smectic mesophases, or reduce/suppress mesomorphism outright if it is an unfavorable location. Reported here is the systematic investigation of using fluorine as lateral substituents within a core-only (or side-chain free) calamitic structure, where each (hetero)aromatic ring is sequentially fluorinated (partially and/or fully) to see the resulting impact that these groups have on observed properties, such as phase transition temperatures, types of mesophases, and electrooptical behaviour. A comparative analysis was conducted to rationalize resulting trends in mesomorphism, and are based on polarized optical microscopy, thermal analysis, variable temperature powder XRD, single crystal structures, and predictions of geometric/electronic/energetic properties obtained from computational calculations (DFT). The absorption/emission properties of these all-aromatic structures in solution and the solid-state are also reported to determine the effect that fluorine substitution has on the frontier orbitals involved in these processes. Included are variable temperature fluorescence experiments to examine how fluorescence changes with temperature and within different (meso)phases. Reported are the lowest transition temperatures for core-only calamitic liquid crystals with a crystallization temperature of 130 °C and a clearing temperature of 214 °C, both of which are suitable for device fabrication.

Received 8th July 2025,
Accepted 3rd October 2025

DOI: 10.1039/d5tc02621k

rsc.li/materials-c

Introduction

Despite the large number of reported calamitic liquid crystals (LCs), only a few core-only (side-chain free) calamitic LCs have been reported and their molecular design and properties are little understood.[1–6] These core-only LC materials are desired not only to gain a better fundamental understanding of what structural/electronic features are required for mesomorphism to emerge in the absence of side-chains (nanosegregation), but their removal should also improve charge transport properties when these conjugated materials are used as an organic semiconductor for organic electronic devices. This is reasoned by the molecules being able to pack closer together as they are free of insulating layers of side-chains and more tolerant to the presence of structural defects (traps). Recently, we reported on the development of a rational molecular design for core-only calamitic LCs based on the **BoBTTX** structure as a molecular template (Fig. 1).[7] These compounds display enantiotropic nematic (N) and/or smectic A phases (SmA) so long as the X-group of the terminal thiophene is an atom or group other than H. Unfortunately, the melting temperatures for these crystalline **BoBTTX** compounds are still high (>180 °C) for use as a mesomorphic organic semiconductor[8,9] through alignment of their crystalline phases by crystallization of their aligned LC phases. Alignment and domain sizes may also benefit from higher order smectic mesophases (*e.g.* SmB and CryE)[10,11] that were not observed for any of the reported **BoBTTX** derivatives.

Studied here is the attachment of one or several fluorine atoms to lateral positions of the benzoxazole (**Bo**), benzene (**B**), and bithiophene (**TT**) parts of the **BoBTTX** template and their effect on intermolecular interactions (phase transition temperatures and types of mesophases), and electronic properties (Fig. 1). Because of its unique properties, fluorine atoms have been incorporated in all types of liquid crystals (LCs),[12–15]

[a] Department of Chemistry and Biochemistry, University of Windsor, Windsor, Ontario N9B3P4, Canada. E-mail: eichhorn@uwindsor.ca
[b] Department of Chemistry, Université de Montréal, 1375 Avenue Thérèse-Lavoie-Roux, Montréal, Quebec H2V 0B3, Canada

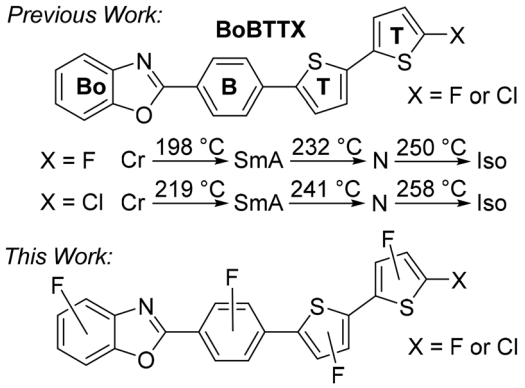

Fig. 1 Previously established molecular template **BoBTTX** for core-only calamitics and its phase transition temperatures for the examples X = F or Cl. Reported here is a large set of fluorinated **BoBTTX** derivatives with X = F and Cl that are expected to have lower transition temperatures and display higher order smectic mesophases, such as smectic C and B, than the **BoBTTX** without lateral fluorine substituents.

especially calamitic LCs.[16–20] Fluorine is the sterically smallest available group/atom after hydrogen, the most electronegative and least polarizable element, and its bond with carbon is very strong and dipolar.[13,20–24] Fluorine has been attached to LCs as electron withdrawing group (*e.g.* CF_3), as fluorinated alkyl chain for nanosegregation, as the polar part of linking and chiral groups, and as a lateral substituent of aromatic core structures to regulate intermolecular interactions (mesophase type and transition temperatures).[12,13,21] A lateral fluorine group attached to the conjugated system can also provide desired modifications to physical (viscosity) and electronic (dielectric, optical) properties of a LC.[13,25] Its highly polar C–F bond generates strong local dipoles that are transverse with respect to the long axis of the molecule.[13] Transverse dipoles facilitate molecular tilting for the generation of tilted smectic phases, especially the smectic C phase that has importance in producing ferroelectric LCs that are highly desirable for use in photonic and display applications.[26] Contrastingly, the low polarizability of fluorine tends to cause weaker intermolecular interactions, and is why fluorine is not commonly used as a terminal substituent in calamitic LCs.[13,14]

What dictates the overall outcome of lateral fluorine substitution is the number of fluorine atoms used and their location within the mesogenic core. Fluorine groups adjacent (*ortho*) to terminal functional groups (fluorine[27,28] or nitrile[29,30] for example) or alkoxy side-chains[31,32] cause small to no decreases to phase transition temperatures when one fluorine is used and no further lowering of the melting point resulted when a second fluorine group is placed at the other *ortho* position so that the lateral dipoles become cancelled. These substitution patterns support and even induce SmA, SmC, and higher order smectic mesomorphism.[25,31,33] In contrast, placing a fluorine group *ortho* to the bond or linking group between two aromatic rings increases the dihedral angle between the conjugated rings, which disrupts π–π stacking interactions and tends to lower transition temperatures.[13,34,35] Still, studies on terphenyl derivatives have shown that lateral fluorination of the inner

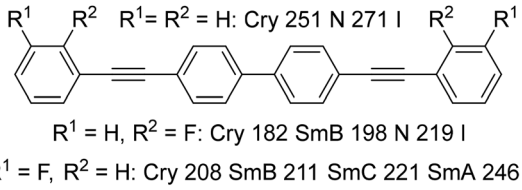

Fig. 2 Core-only tolane oligomers with phase transition temperatures in °C.[6]

phenyl ring with two fluorine atoms on the same side support higher order smectic C and B mesophases.[3,13,17,34,36]

One example on how core-only tolane oligomers benefit from lateral fluorination was reported by Twieg *et al.* (Fig. 2).[6] The non-fluorinated tolane oligomer exclusively displays nematic mesomorphism, whereas the oligomer with fluorine *ortho* to the acetylene group displays SmB and N mesophases, and the *meta* derivative supports SmA, SmC, and SmB mesomorphism. Clearly, lateral fluorination benefits their mesomorphism likely because steric hindrance is small and the transverse dipoles increase intermolecular interactions to a degree that smectic (lamellar) mesomorphism emerges.

The systematic study presented here widely varies the number and location of the fluorine atoms across all three parts of the **BoBTTX** template to probe where exchange of hydrogen for a fluorine has a beneficial or detrimental effect on the mesomorphism of these derivatives and core-only calamitics in general. Also reported are changes to the absorption and emission properties between fluorinated and non-fluorinated derivatives and the dependence on the location of the fluorination.

Results and discussion

Design and synthesis

The library of partially fluorinated calamitic core-only structures to be studied can be subdivided into three different categories: (i) partial or full fluorination of the thienyl and bithienyl parts (**TF_3**, **TTF_3**, **TF_2TF_3**, and **TF_2T-X** (X = F or Cl)); (ii) partial fluorination of the inner benzene ring (**BF2-X**, **BF3-X** and **BF23-X** (X = F or Cl)); and (iii) partial or full fluorination of the benzene ring of benzoxazole (**FoBo-X**, **FnBo-X**, **FFBo-X** and **4FBo-X** (X = F or Cl)). Acronyms are devised according to the following: **Bo** = benzoxazole, **B** = benzene, **T** = thiophene, whilst the regiochemical designations for where the fluorine groups are located on the inner benzene ring and benzoxazole's benzene ring are used for labelling for the last two categories of compounds as all other components of the molecule are identical. Both fluorine and chlorine substituents were chosen to serve as the terminal functional group to ensure that the observed trends resulting from lateral fluorination were consistent between different terminal functional groups.

The connected series of conjugated rings in these core-only structures were sequentially attached using a combination of Stille cross-coupling, annulation and/or direct arylation chemistry. Stannyl fluorinated thiophene intermediates were

synthesized using lithiation for electrophilic substitution by fluorine from *N*-fluorobenzenesulfonimide (NFSI). This was followed by tributyltin chloride, all according to a literature procedure from Sakamoto *et al.*, which generated 2-tributylstannyl-3,4,5-trifluorothiophene in an overall yield of 57% over four steps and 5-tributylstannyl-perfluorobithiophene in an overall yield of 3% over six steps (the yield suffers a substantial drop during the Stille coupling of the two fluorinated thiophenes).[37] One deviation from the synthetic protocols provided by Sakamoto *et al.* involved the trimethylsilyl-perfluorobithiophene intermediate that precedes the stannylated version of this compound, as it underwent deprotection during column chromatography. So, the intended replacement of the trimethylsilyl group for bromine followed by tributyltin was not followed.[37] Instead, stannylation *via* lithiation of obtained 3,3′,4,4′,5-pentafluoro-2,2′-bithiophene was done for electrophilic addition of tributyltin chloride to give the desired stannylated intermediate. Finally, generation of 2-tributylstannyl-5-chlorothiophene was done using the same process of lithiation for electrophilic addition of tributyltin chloride and was obtained in an excellent yield of 90%. All synthetic protocols discussed above and to be shown are given with further details as SI.

The synthetic pathways followed for generating the partially or fully fluorinated bithienyl set of core-only structures is presented in Scheme 1. The first step involved generating benzoxazole *via* a copper catalyzed domino annulation reaction from an established literature procedure[38] to give **1** in a yield of 69%, which is 30% less than what is reported, with the loss of conversion attributed to an unoptimized scale up of approximately 40 times. Four synthetic pathways branched off from this intermediate, but all involved a Stille cross-coupling of a stannylated (bi)thiophene as the next step, as coupling of 2-tributylstannyl-3,4,5-trifluorothiophene or 5-tributylstannyl-perfluorobithiophene with **1** in the microwave synthesizer (which is used regularly herein to decrease required reaction times) at 140 °C for two hours gave final products $\mathbf{TF_3}$ and $\mathbf{TF_2TF_3}$ in yields of 49% and 30% respectively (overall yields of 34% and 21%). Attachment of unfunctionalized thiophene *via* Stille cross-coupling to **1** at reflux in toluene (hot stir plate) produced intermediate **2** in 79% yield, which was then brominated *via* electrophilic aromatic substitution using *N*-bromosuccinimide in a chloroform/acetic acid mixture under reflux to give intermediate **3** in 90% yield. Finally, Stille cross-coupling between **3** and 2-tributylstannyl-3,4,5-trifluorothiophene using regular microwave synthesizer reaction conditions (140 °C for 2 hours) was performed to give $\mathbf{TTF_3}$ in a yield of 48% (overall yield of 24%). The remaining $\mathbf{TF_2T\text{-}X}$ compounds would be made in a similar manner to $\mathbf{TTF_3}$, except that the first Stille coupling reaction involved a stannylated difluorothiophene intermediate protected with a trimethylsilyl (TMS) group being coupled to **1** using the same reaction conditions as to obtain **2** to give intermediate **4** in a yield of 57% (22% lesser conversion for **4** when compared to **2**). From here, deprotection of the TMS group using tetrabutylammonium fluoride (TBAF) gave intermediate **5** quantitatively, and remaining steps of bromination and Stille cross-coupling (using either a fluorine or chlorine terminated thiophene) used identical reaction conditions as done to obtain **3** and $\mathbf{TTF_3}$ to give $\mathbf{TF_2T\text{-}F}$ and $\mathbf{TF_2T\text{-}Cl}$ in an overall yield of 11% for each compound.

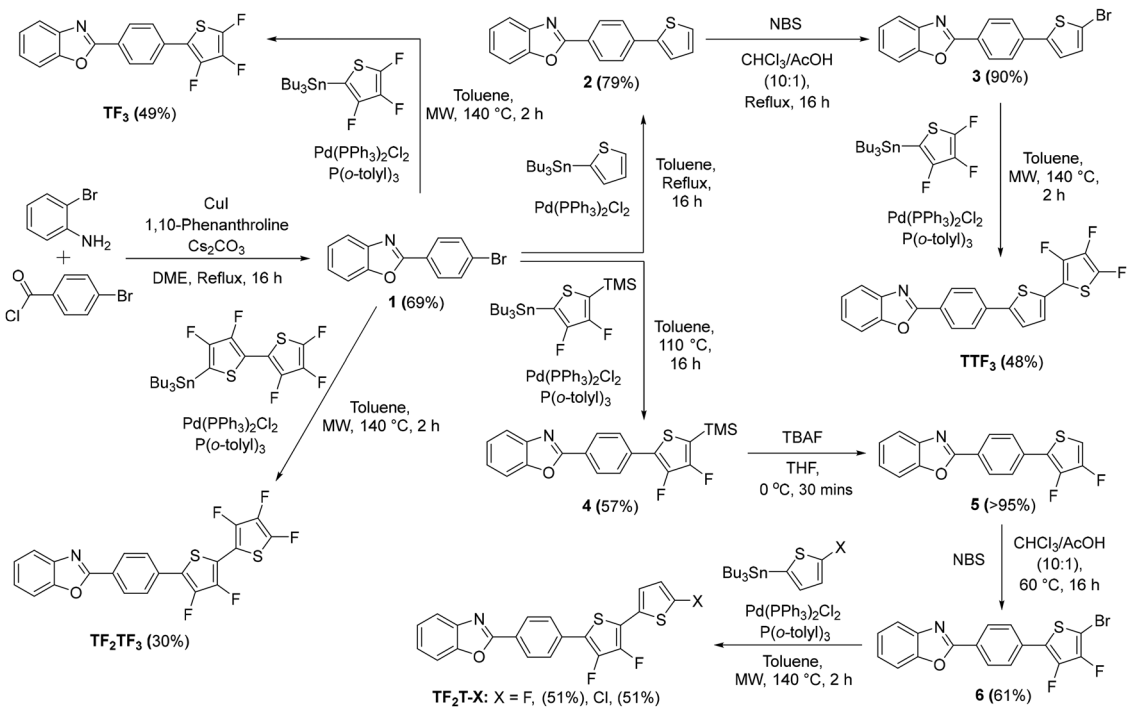

Scheme 1 Synthetic route for core-only calamitics with the bithiophene moiety partially or fully fluorinated, consisting of $\mathbf{TF_3}$, $\mathbf{TTF_3}$, $\mathbf{TF_2TF_3}$ and $\mathbf{TF_2T\text{-}X}$ (X = F or Cl).

It is hypothesized that inductively electron withdrawing fluorine groups are deactivating the transmetallation of the aryl group onto the palladium center (especially when *ortho* to the stannyl group), in Stille couplings. This hinders the effectiveness of the cross-coupling reaction and gives lower yields when compared to Stille couplings with unfunctionalized stannylated thiophene (average yields of 50–60% when using stannylated fluorothiophenes compared to stannylated thiophene where average yields are 70–80%).[39–41]

The synthetic pathways followed to generate the set of compounds where the inner benzene ring (**B**) is mono- or di-fluorinated are outlined in Scheme 2. For the mono-fluorinated derivatives, 4-bromo-(2 or 3)-fluorobenzoic acid was converted quantitatively to an acid chloride using oxalyl chloride according to a literature procedure[42] so that the same copper catalyzed annulation reaction[38] could be done to form the benzoxazole ring, giving compounds **8** and **12** in yields of 53% and 85% respectively. The lower yield obtained for compound **8** is attributed to decreasing electron density on the aromatic carbon that the acid chloride is attached to *via* inductive effects from the *ortho* fluorine substituent. The inductive effect lowers the ability of the oxygen of the carbonyl group from coordinating to the cooper metal and performing the reductive elimination step. This reduced reactivity is more prevalent the closer the fluorine substituent is to the acid chloride, as the yield for compound **12** (fluorine substituent is *meta* with respect to the acid chloride) remained high. Next, addition of a thiophene ring to **8** and **12** was accomplished *via* Stille cross-coupling of 2-tributylstannylthiophene at 110 °C to give intermediates **9** and **13** in yields of 87% and 76% respectively. Achieving equivalent four ring compound **16** (relative to **9** and **13**) but with a difluorinated benzene ring was done over two steps, starting with 1,4-dibromo-2,3-difluorobenzene being statistically mono-substituted with thiophene *via* a Stille cross coupling reaction with 2-tributylstannylthiophene under typical microwave synthesizer reaction conditions (except for a one hour increase to reaction time to 3 hours), giving intermediate **15** in 58% yield. This was followed by a palladium-copper co-catalyzed direct arylation reaction between **15** and benzoxazole using a modified procedure from Huang *et al.*[43] (reaction temperature and solvent changed from 100 °C to 140 °C and toluene to DMF) to give di-fluorinated compound **16** in 44% yield. Remaining synthetic steps to achieve the target final products are the same from this point regardless of the degree of fluorination of this inner benzene ring, as bromination of thiophene was accomplished *via* previously established electrophilic aromatic substitution using NBS (yields ranged from 57% to 75%) and attachment of the terminal fluoro or chlorothiophene *via* Stille cross-coupling of the appropriately functionalized stannylated thiophene under typical microwave reaction conditions gave the six final compounds **BF2-F**, **BF2-Cl**, **BF3-F**, **BF3-Cl**, **BF23-F** and **BF23-Cl** with coupling yields ranging from 50% to 85% and overall yields ranging from 13% to 33% for mono-fluorinated compounds over five steps and 13% for di-fluorinated compounds over four steps.

The last sets of synthesized compounds were those with the benzene ring on benzoxazole being either mono-, di- or fully fluorinated and outlined synthetic pathways are given in Scheme 3. The same sequence of reactions followed for generating $\mathbf{TTF_3}$, **BF2-X** and **BF3-X** were employed for generating the mono- and di-fluorinated **FoBo-X**, **FnBo-X** and **FFBo-X** compounds; (1) domino annulation reaction; (2) Stille cross coupling of 2-tributylstannylthiophene; (3) bromination *via* NBS; and (4) Stille cross-coupling of the terminal fluoro- or chlorothiophene. Similar ranges of yields were obtained for each synthetic step after the initial domino annulation reaction, with one exception being the poor yield obtained during the final coupling reaction to produce **FFBo-Cl**, which is expected to give a comparable yield to its fluorine counterpart when optimized. Overall yields for these three sets of compounds were calculated between 16% and 39% over four steps (this excludes the aforementioned poor final coupling obtained when synthesizing **FFBo-Cl**). The first synthetic step will be discussed in more detail as the position of the fluorine

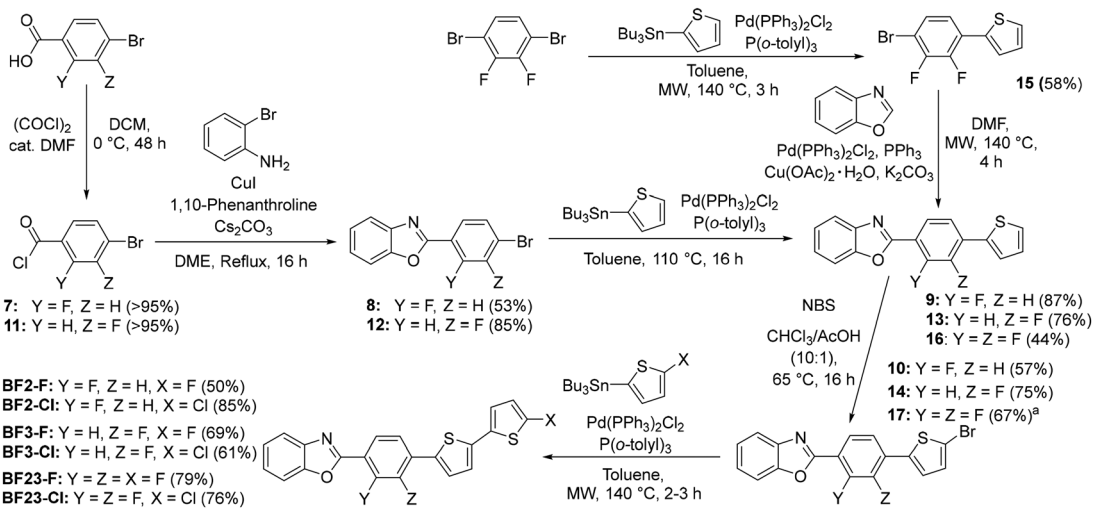

Scheme 2 Synthetic route for core-only calamitics with the inner benzene ring partially fluorinated, consisting of **BF2-X**, **BF3-X**, and **BF23-X** (X = F or Cl). [a] DMF at 80 °C was used instead of $CHCl_3$/AcOH.

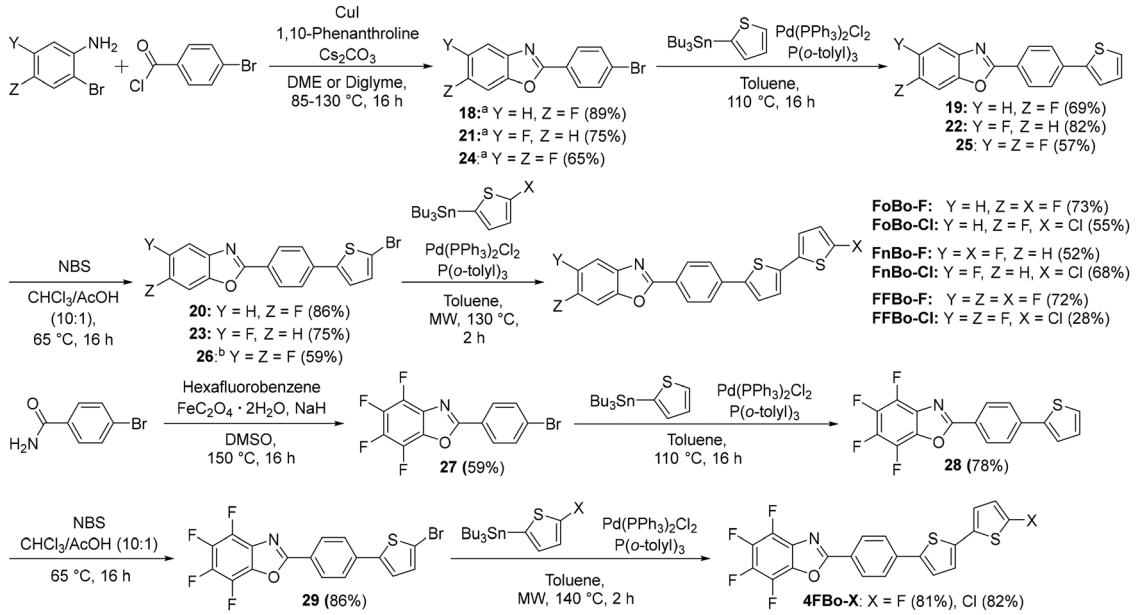

Scheme 3 Synthetic route for core-only calamitics with the benzene ring of benzoxazole partially or fully fluorinated, consisting of **FoBo-X**, **FnBo-X**, **FFBo-X** and **4FBo-X** (X = F or Cl). [a] **18** was achieved using DME at reflux, while **21** and **24** were achieved using diglyme at 120 °C and 130 °C, respectively. [b] Reaction conditions vary from what is shown, as DMF/acetic acid (10 : 1) at 85 °C was used instead.

substituent on the bromoaniline starting material had a significant yet predictable effect on the efficiency of the annulation reaction. When the fluorine substituent is *para* to the carbon bearing the amine group (used to make **18**), it is as far away from the amine as possible, thereby minimizing any deactivation of the amine as a nucleophile from inductive effects by proximity, while resonance (or mesomeric) effects serve to activate the amine group (*para* substitution of a π-donating group). These effects collectively permit a high yield (89%) to be realized for **18**. However, when the fluorine substituent is *meta* to the amine group (used to make **21**), deactivation by inductive effects and no activation from resonance effects hinders the effectiveness of the amine as a nucleophile for the condensation step, and resonance effects of the *para* π-donating fluorine also reduce the reactivity of the carbon bearing the bromine group. This explains why a higher boiling solvent was needed (exchange of dimethoxyethane to diglyme) as higher temperatures (85 °C to 120 °C) were required to overcome these deactivating factors, giving **21** in a lesser but still good yield of 75%. Finally, domination of inductive effects dictated a reduced reactivity of bromoaniline when two fluorine substituents are present, which explains how a 10% lower yield is obtained when going from mono-fluorinated **21** to difluorinated **24** even though a 10 °C increase in reaction temperature was performed.

Finally, the last set of compounds, **4FBo-X**, used a different first synthetic step than what has been presented thus far, as a two fold nucleophilic aromatic substitution reaction between benzamide and hexafluorobenzene in DMSO at 150 °C produced intermediate **27** in 59%, which was comparable to what was obtained in the associated followed literature procedure.[44] From here, all synthetic steps are identical to what has been shown for most of these sets of fluorinated calamitic structures (Stille cross-coupling of 2-tributystannylthiophene, bromination, then final Stille cross-coupling of fluoro or chlorothiophene) and were obtained in comparable or slightly higher yields to give final products **4FBo-F** and **4FBo-Cl** in an overall yield of 32% for each compound.

Mesomorphism

The mesophase types with their associated phase transition temperatures and enthalpies for all core-only fluorinated calamitics are summarized in Fig. 5, 6 and 8 and Fig. S9, S10 and S11. They were determined through polarized optical microscopy (POM), differential scanning calorimetry (DSC), and variable temperature powder X-ray diffraction (vt pXRD) characterization. Characteristic Schlieren and focal-conic fan textures were observed for nematic (N) and smectic A (SmA) mesophases, respectively. Some compounds showed large domains of spontaneous planar (homogeneous) alignment within the N and SmA mesophases when sandwiched between untreated glass slides (Fig. 3a). Planar alignment was also observed by vt pXRD experiments, where the long axes of the molecules arranged themselves planar to the glass surface and with an approximate angle of 22° between the smectic layer normal and the long axis of the capillary. The alignment helped confirm the SmA character for all the observed lamellar mesophases, as the 2D pXRD images demonstrate a 90° angle between the reflections of layers (longitudinal) and reflections of the lateral packing of the molecules (equatorial) (Fig. 4b and Fig. S33). The most intense reflection observed within the SmA pXRD patterns is designated as the (100) reflection and representative of the average layer spacing in the lamellar mesophase. Often a weak second order (200) reflection and even

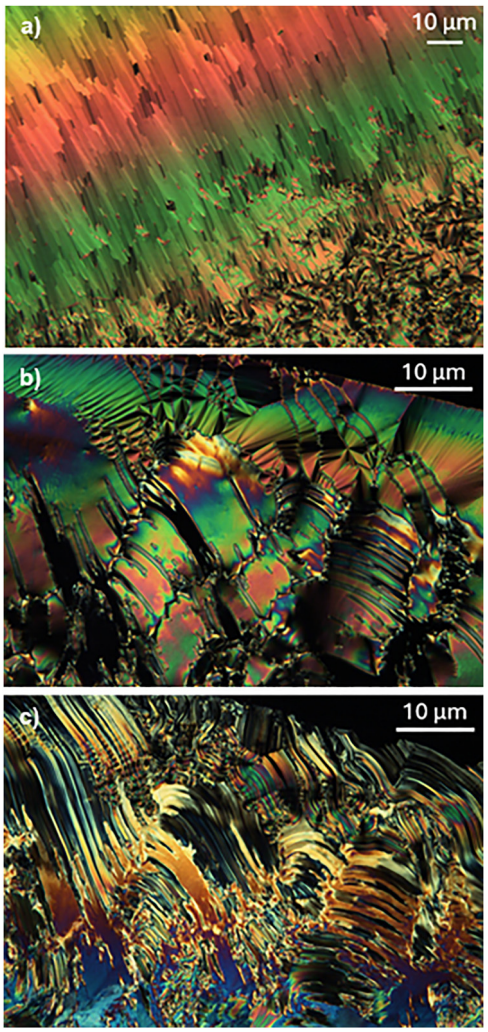

Fig. 3 Polarized micrographs (crossed polarizers) of (a) **BF23-F** at 158 °C on cooling showing spontaneous alignment (homogeneous) within the smectic A phase (fan-shaped texture); (b) **FoBo-F** at 278 °C on cooling showing the smectic A phase (fan-shaped texture); and (c) crystalline phase of **FoBo-F** at 178 °C on cooling showing the imprinting of the prior mesophase's texture during crystallization.

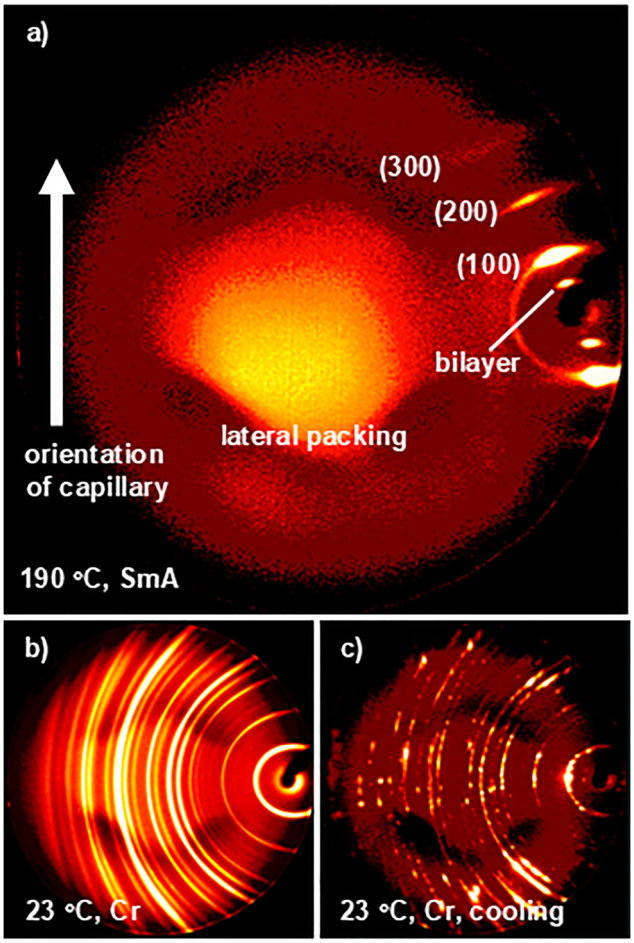

Fig. 4 2D vt pXRD images of **BF3-Cl** at (a) 190 °C on first heating in the SmA phase showing its propensity for spontaneous alignment; (b) 23 °C in the crystalline phase obtained by precipitation from solution; and (c) 23 °C on cooling into the crystalline phase obtained by crystallization from the aligned SmA phase. The intense diffraction spots in the diffraction pattern of (c) indicate the formation of larger crystalline domains than by crystallisation from solution in (b).

some third order reflections of the layer spacing are also observed. For all smectic compounds the *d*-spacing of the (100) reflection is approximately equal to the length of the molecules, which was estimated by determining the lowest energy conformer by DFT calculations and adding the atomic radii of the two atoms used for measuring the length (Tables S4 and S10). For example, the (100) reflection of **BF3-Cl** in its SmA phase has a *d*-spacing of 20.9 Å while its molecular length was calculated to be 20.4 Å. This sample also gives a small angle reflection at a *d*-spacing value of 41.0 Å, which is roughly twice the spacing of the (100) reflection and likely indicates bilayer formation with the X groups being in the centre. Additionally, molecular widths and π–π stacks make up the broad reflections for the lateral packing that were found between 3.5 to 5.0 Å.

Crystallization of the SmA phases often occurs without large changes to the domain structure and alignment of the preceding SmA phase, as can be concluded from POM images of compound **FoBo-F** (Fig. 3c and d). This provides the prospect of aligning crystalline phases *via* the alignment of preceding SmA phases. In addition, 2D pXRD patterns (Fig. 4a, c, and Fig. S42) reveal an increase in domain sizes for the crystalline phase obtained from the SmA phase (Fig. 4c) when compared to the p-XRD pattern of the crystalline phase obtained by precipitation from solution (Fig. 4a).

Mesomorphism of compounds with partially or fully fluorinated bithiophene parts, reference compound **BoBTTF**, and compound $\mathbf{TF_3}$ is presented in Fig. 4. The shorter, four-ring structure $\mathbf{TF_3}$ displayed no LC character as a result of insufficient aspect ratio (2.6 compared to five-ring structures that are greater than 3.1). Full fluorination of the terminal thiophene in $\mathbf{TTF_3}$ retained the SmA and N phases that were observed in reference compound **BoBTTF** and only marginally affects phase transition temperatures and enthalpies, except for the 50% larger melting enthalpy for $\mathbf{TTF_3}$. Apparently, using a

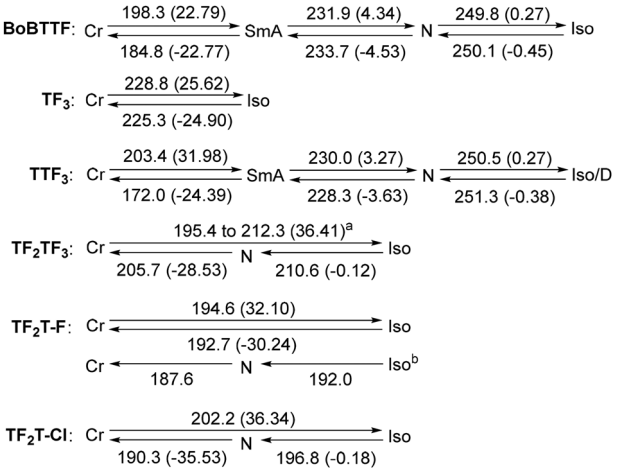

Fig. 5 Phase transition temperatures (°C) and (enthalpies (kJ mol^{-1})) of derivatives with the bithiophene moiety (**TT**) partially or fully fluorinated. Values are determined by DSC at 5 °C min^{-1} under N_2 for 2nd-heating and 1st-cooling runs. Cr = crystalline phase; SmA = smectic A; N = nematic; Iso = isotropic liquid; D = decomposition. [a] Broad melting transition with several overlapping peaks; Values given are the onsets of the transitions for the first and last thermal event. [b] Observed only by POM at high cooling rates >20 °C min^{-1}.

5-fluorothiophene or 3,4,5-trifluorothiophene as the terminal ring overall does not significantly alter the intermolecular interactions of these two compounds in their crystalline and mesophases. DFT calculations (Table S12) predict a 2.5 kJ mol^{-1} lower rotational barrier between the two thiophene rings in **TTF$_3$** when compared to **BoBTTF**, which should lower transition temperatures but must be compensated for by stronger dipole–dipole and donor–acceptor interactions in **TTF$_3$**. However, the high electron density at the terminal thiophene when it is fully fluorinated in **TTF$_3$** leads to a decrease in thermal stability since the compound starts decomposing once it reaches its clearing point of 250 °C while **BoBTTF** does not.

In contrast, difluorination of the inner thiophene in compounds **TF$_2$T-F**, **TF$_2$T-Cl**, and **TF$_2$TF$_3$** disrupts mesomorphism with only short-range monotropic N phases being left. This loss in enantiotropic mesomorphism must be caused by intermolecular interactions specific to the LC phases since the melting points of all three compounds do not significantly change when compared to **BoBTTF** and **TTF$_2$**. Examination of electronic properties or rotational energy barriers within these compounds does not reveal any obvious reasoning as to why these losses of enantiotropic mesomorphism transpires. It is hypothesised that incorporating these lateral substituents within the ring that provides the molecular kink in the middle of the **BoBTTX** structure causes significant enhancement of the effective kinking that disfavours close lateral packing in the LC phases. This is supported by the observation that lateral *ortho* difluorination of the benzene ring retained enantiotropic SmA and N behaviour (see below). One observation that can be made here is that the temperatures at which the monotropic nematic mesophases appear decrease when fewer and smaller functional groups are found on the terminal thiophene.

Introducing fluorine substituents within the inner benzene ring of the **BoBTTX** template reduces the thermal stability of all displayed phases, although the temperature ranges of the enantiotropic N and SmA phases significantly increases (Fig. 6). The crystalline and mesophases are most destabilized in **BF2-X** (the crystalline phase by more than 60 °C and 70 °C compared to **BoBTTF** and **BoBTTCl**, respectively) followed by **BF23-X** and **BF3-X**. Clearly, the fluorine *ortho* to the benzoxazole moiety is much more disturbing for the crystalline and mesophases than the fluorine *ortho* to the thiophene moiety. This may be reasoned with a higher degree of coplanarity between fluorobenzene and thiophene in **BF3-X** than between benzoxazole and benzene in **BF2-X** because of steric hindrance. In general, the destabilizing effect of lateral groups decreases with decreasing degree of order of the phase. Consequently, the N mesophases should be less destabilized by the lateral fluorine groups than the SmA phases and the crystalline phases are most destabilized. Indeed, this is what is observed in this set of fluorinated compounds and results in a widening of the temperature ranges of the N phases and no change or shrinking of the temperature ranges of the SmA phases.

A possible reason for these large decreases in phase transition temperatures for compounds **BF2-X** is the predicted decrease in rotational energy barrier between benzoxazole and the inner benzene to half the value (from 28 to 14 kJ mol^{-1}, Table S12). Although a coplanar orientation remains the most stable conformation in the gas phase according to DFT calculations, the energy of the coplanar conformation is increased when the benzene ring is fluorinated at its *ortho*-position. This can be rationalized with greater steric repulsion between the fluorine and the oxygen/nitrogen of benzoxazole. However, the contribution of other electronic factors that would lower the rotational barrier of this bond cannot be excluded. Finally, the destabilization of

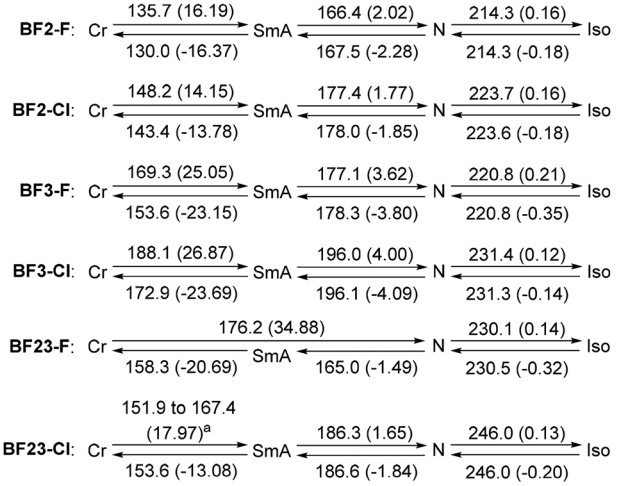

Fig. 6 Phase transition temperatures (°C) and (enthalpies (kJ mol^{-1})) of derivatives with the inner benzene ring (**B**) partially fluorinated. Values are determined by DSC at 5 °C min^{-1} under N_2 for 2nd-heating and 1st-cooling runs. Cr = crystalline phase; SmA = smectic A; N = nematic; Iso = isotropic liquid. [a] Broad melting event with several transitions; values given are the onsets of the transitions for the first and last thermal event.

especially the crystalline phases agrees with the smaller melting enthalpies of 13–16 kJ mol^{-1} compared to 20–45 kJ mol^{-1} for all other fluorinated **BoBTTX** derivatives reported here (Fig. S10, S11 and S12).

Fluorination at the 3-position for **BF3-X**, in comparison, does not lower phase transition temperatures as low as in **BF2-X**. Most notably, the melting points of **BF3-F** and **BF3-Cl** are 33 °C and 40 °C higher than for **BF2-F** and **BF2-Cl**, respectively, which still is 29 °C and 31 °C lower than for the corresponding reference compounds **BoBTTF** and **BoBTTCl**, respectively. In contrast, the SmA phases of **BF3-F** and **BF3-Cl** are only 11 °C and 19 °C more stable than for their **BF2-X** counterparts and the nematic phases are stabilized by only 7 °C. This results in reduced temperature ranges for SmA and, much less so, N mesophases in **BF3-X** when compared to **BF2-X**. Consequently, the fluorobenzene *ortho*-connected to a thiophene in **BF3-X** is a less disturbing structural unit than the fluorobenzene *ortho*-connected to a benzoxazole group in **BF2-X**, especially for their crystalline phases. This agrees with reports on conventional calamitics where fluorobenzene *ortho*-connected to a benzoxazole diminishes phase transition temperatures much more so than when *ortho*-connected to a thiophene (Fig. 7a (ref. 45 and 46) and Fig. 7b (ref. 31 and 47)). The decreased propensity for lamellar mesomorphism in **BF3-X** is reasoned with a 30° dihedral angle between the benzene and thiophene rings caused by greater steric hinderance between the fluorine substituent and the thienyl hydrogen, which has also been reported for conventional calamitics (Fig. 7b). In contrast, the DFT predicted increase for the rotational energy barrier between *ortho*-fluorobenzene and thiophene by 2.5–3 kJ mol^{-1} (Table S12) does not significantly increase the thermal stability of the SmA phase.

Attachment of two fluorine atoms to the inner benzene ring in **BF23-X** was expected to have the combined effect of **BF2-X** and **BF3-X**, but a further destabilization of the crystal and mesophases is not observed but was reported for conventional calamitics (Fig. 7c[13,35,48]). Both crystalline and N phases increase in stability for **BF23-F**, whereas the SmA phase is reduced to a monotropic mesophase. A similar behaviour is shown by **BF23-Cl** although the SmA phase is 20 °C more stable than for **BF23-F** and remains enantiotropic. Overall, exchanging the terminal X group from F to Cl increases the phase transition temperatures by 10 to 16 °C. The higher transition temperatures of the chlorinated compared to the fluorinated compounds are likely caused by their large differences in space-filling and polarizability. However, comparison between molecular electronic properties did not provide more evidence that helped explain any of the observed mesomorphic trends. For example, the dipole moments between **BF2-X**, **BF3-X**, and **BF23-X** varied from 0.72 to 3.12 D without showing a specific trend for their mesomorphism. Additionally, the dipole moment of 3.12 D for the lowest energy conformer of **BF3-Cl** dropped by up to 1 D for other conformers that are only 0.2 kJ mol^{-1} higher in energy. Increasing polarizability anisotropy has been generally correlated with increased nematic phase ranges,[25,31,49] which agrees with **BF23-X** having the highest values, whereas the average polarizability was consistent across these six fluorinated benzene derivatives. Finally, the examples given in Fig. 7 all report the induction of a SmC phase upon fluorination, a phenomenon that was not observed for any of the core-only liquid crystals presented here.

Benzoxazole's benzene ring was mono- di- and tetrasubstituted with fluorine to probe the effects on mesomorphism in comparison to non-fluorinated reference compounds **BoBTTF** and **BoBTTCl** (Fig. 8). **FnBo-X** and **FoBo-X** are monofluorinated in *meta*-position to the oxazole N and oxazole O, respectively. These positions barely influence the length and width (aspect ratio) of the molecules and should not be considered as lateral groups. Consequently, incorporation of one fluorine in *meta*-position was expected to have little affect on the phase transition temperatures, which is what is observed for the melting/crystallization and SmA to N transitions when compared to **BoBTTX**. The melting points for derivatives with chlorine as terminal X group are 5 to 25 °C higher than for X = F, as for all other derivatives, and the SmA phases of **FnBo-X** and **FoBo-X** are stabilized by 8 to 23 °C. Significantly higher by 50 to 70 °C are the clearing temperatures (N to isotropic liquid) of **FnBo-X** and **FoBo-X** when compared to **BoBTTX**.

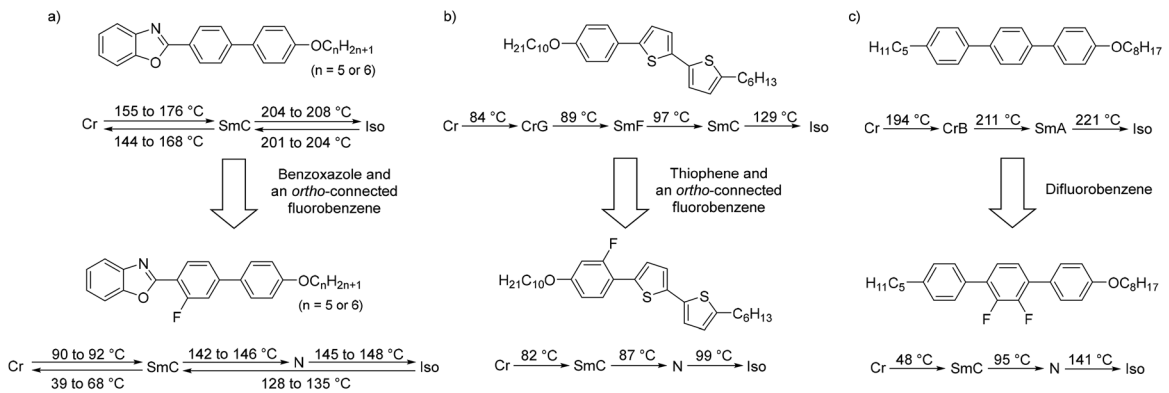

Fig. 7 Comparison between fluorinated and non-fluorinated inner benzene rings within calamitic LCs with side-chains, where fluorine substituted *ortho* to benzoxazole (a),[45,46] thiophene (b),[31,47] or difluoro substitution (c)[13,35,48] was comparatively assessed to equivalent structures without these lateral fluorine substituents.

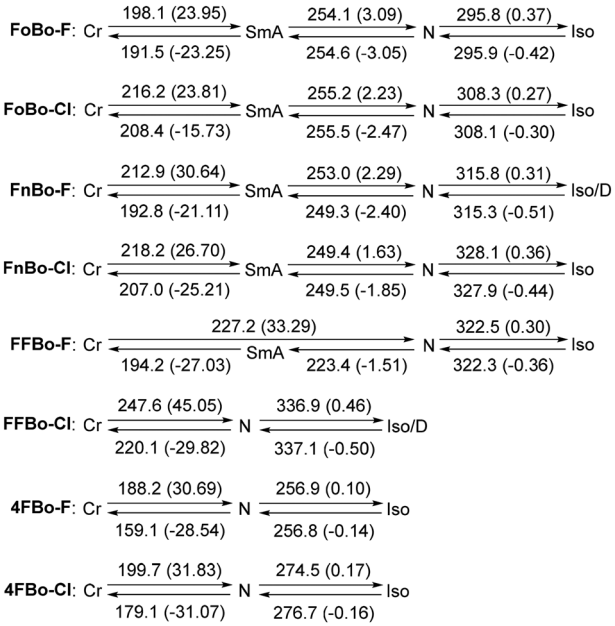

Fig. 8 Phase transition temperatures (°C) and (enthalpies (kJ mol^{-1})) of derivatives with the inner benzoxazole (**Bo**) partially and fully fluorinated. Values are determined by DSC at 5 °C min^{-1} under N_2 for 2nd-heating and 1st-cooling runs. Cr = crystalline phase; SmA = smectic A; N = nematic; Iso = isotropic liquid; D = decomposition.

The reasons for this large increase in nematic phase stability remain unclear but it is by about 20 °C more pronounced for **FnBo-X** than for **FoBo-X**. Exchanging the location of fluorine from being *meta* to nitrogen instead of oxygen causes an average increase to the dipole moment by 1.6 D (0.58–0.76 D to 2.06–2.43 D from **FoBo-X** to **FnBo-X**, Table S11), and an increasing dipole moment strength has been previously correlated with increased phase transition temperatures and nematic phase stabilization due to greater dipole–dipole intermolecular interactions.[45,50] Rotational energy barriers between benzoxazole and the inner phenyl ring remain consistent regardless of the degree of fluorination and the monofluorination does not lower the symmetry of the compounds, which would have lowered transition temperatures especially of the melting process.[51]

Substitution of both *meta*-positions of the benzoxazole with fluorine gives compounds **FFBo-X** that display more stable crystalline phases by 30 to 34 °C compared to **BoBTTX** and their nematic phases are stable to 322 °C and >337 °C before decomposition starts. Clearing temperatures of **FFBo-X** exceed those of **FoBo-X** and **FnBo-X** as greater longitudinal dipole moments were calculated for these difluorinated structures (denoted as the *x*-component of the dipole moment within Table S11). In contrast, the SmA phases of **FFBo-X** are destabilized by about 10 to 30 °C compared to **BoBTTX**, **FoBo-X**, and **FnBo-X** that causes **FFBo-F** to exhibit only a monotropic SmA phase while the SmA phase is altogether suppressed within **FFBo-Cl**. Clearly, the two fluorine atoms increase intermolecular interactions in the solid and nematic phases but support smectic mesomorphism to a much lesser degree. This is contrary to what we expected for **FFBo-F** as we hypothesised that fluorophilic interactions between the fluorine groups now concentrated at both ends of the molecule could also offer a means to promote lamellar mesophases. In this case, fluorine groups would most strongly interact when molecules organize into layers to generate a nanosegregated interlayer of fluorine atoms, although a sufficiently close packing is difficult to achieve.

Lastly, full fluorination of the benzoxazole in **4FBo-X** now introduces two lateral fluorine atoms in *ortho*-positions to the oxazole ring. Expectedly, melting temperatures decease by 10 to 20 °C compared to **BoBTTX** but, unexpectedly, clearing temperatures of the N phases increase by 8 to 16 °C compared to **BoBTTX** while smectic mesomorphism is completely suppressed in **4FBo-X**. The higher clearing temperatures for **4FBo-F** and **4FBo-Cl** compared to their non-fluorinated counterparts are attributed to the higher dipole moments of the fluorinated compounds (Table S11). This combination of lower melting and higher clearing temperatures generates nematic phases with the widest temperature ranges of about 98 °C for any structure investigated herein.

Single crystal studies

Although molecular conformations and packing structures can significantly differ in the crystalline and liquid crystalline phases, invaluable information about intermolecular interactions and molecular shape can be extracted from single crystal structures and used as a starting point for developing packing models for their mesophases. **TTF$_3$** was the only fluorinated derivative that gave crystals of sufficient quality (Fig. 9). The compound is mostly planar in the crystal phase, which permits effective π–π stacking interactions, yet, these π–π stacks are organized into paired molecular layers, where antiparallel

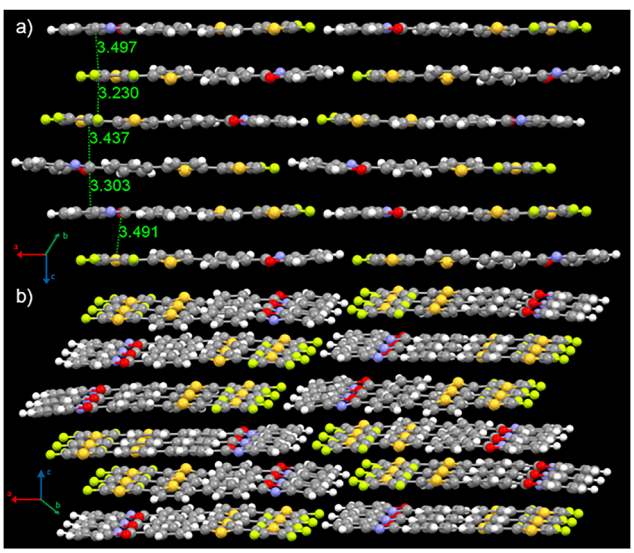

Fig. 9 Single crystal structure of **TTF$_3$**: (a) antiparallel layering between a set of π–π stacked layers, but the π–π stacked layers are laterally offset and rotated by 180° between neighbouring stacked layers from above/below; and (b) molecules orient in a "head to tail" lateral packing style.

orientation is maintained within the paired layer (to offset the longitudinal molecular dipole moment), but the immediate layer above or below has parallel orientation with respect to this paired layer (while being slipped laterally by 1.5–1.6 Å) (Fig. 9a). What this reveals is how the trifluorothiophene components organize molecular packing so that they can remain close to one another between neighbouring molecules so that fluorophilic interactions are affective.[52,53] This is supported by examining the distances between the molecular layers along the π-stacking axis, as the intermolecular distances within the paired π–π stacked layer is 3.4–3.5 Å (the typical distance for π–π interactions), while the intermolecular distance between different paired layers is contracted to 3.2–3.3 Å. This reduced interlayer spacing would be driven by increasing fluorophilic interactions as these fluorinated rings are pushed closer to each other, and compensation for this spatial contraction is done by every other molecular layer twisting its remaining conjugated rings to fill the free space generated from these interacting trifluorothiophene rings. Additionally, changes to the orientation of the inner thiophene ring occurs between paired layers, as the sulfur atoms are still positioned on the same side of the molecule but are oriented towards each other between these paired layers (Fig. 9b). This again occurs due to the desire for fluorophilic interactions as this pushes the trifluorothiophene rings closer to one another between paired layers.

This packing arrangement along the π-stacking axis within **TTF$_3$** contrasts that for previously studied crystal structures of core-only calamitics comprised of the **BoBTTX** molecular building block.[7] These possess consistent antiparallel layering, while a combination of antiparallel and parallel layering exists within **TTF$_3$**. This observational difference is why fluorophilic effects are hypothesized to drive the resulting molecular packing structure of **TTF$_3$**, as they reorient molecules to place the fluorine groups in positions for greater interactions than space filling or symmetry considerations would otherwise dictate. Still, steric considerations involving the replacement of hydrogen atoms by larger fluorine atoms cannot be fully excluded as contributing to the resulting crystal structure for **TTF$_3$**.

Absorption/emission properties

All fluorinated calamitic structures were readily soluble in THF, chlorinated and aromatic solvents and all associated optical data are reported in Table S1. All compounds obeyed the Lambert–Beer's law between concentrations of 10^{-4} to 10^{-7} M and molar extinction coefficients for the longest wavelength absorption ranged from 40 000–50 000 M^{-1} cm^{-1}. Absorption spectra of Fig. 10a and 11 mainly show that fluorine substituents have only a small influence on the optical properties of these conjugated materials in solution as absorption maxima for all five ring structures range from 363–384 nm. More fluorination on the benzene and benzoxazole rings results in maxima at longer wavelengths within this range. This corresponds with estimated optical band gaps that range from 2.8–3.1 eV whilst absorption extended up to 435 nm. Bathochromic shifts of 3–4 nm were observed when exchanging from fluorine to chlorine as the terminal functional group X, indicative of the greater participation by the chlorine substituent with the conjugated system.

The absorption spectrum of **TF$_3$** is expectedly blue shifted by 40–50 nm because it is a smaller conjugated molecule, but the shape of its absorption spectrum is very similar to that of all **BoBTTX** derivatives with fluorinated bithiophene groups. Their longest wavelength absorption peak is not the most intense and appears as a shoulder. It is likely associated with the vibrational ground state of the first excited electronic state (Fig. 10a). This shoulder is not or barely visible for any of the benzene and benzoxazole fluorinated **BoBTTX** derivatives (Fig. 11).

Emission spectra in solution, like absorption spectra, are very similar for all fluorinated derivatives, except for the blue shifted shorter **TF$_3$**. Noticeable differences exist between the fluorinated bithiophenes and the derivatives with fluorinated benzene and benzoxazole units. Emission spectra of the latter are wider (about 200 nm at the baseline) and the longest wavelength emission is the most intense vibrational mode (Fig. 11). Emission spectra of the former are somewhat narrower (175 nm at the baseline) and the shortest wavelength emission is the most intense vibrational mode except for **BoBTTF** (Fig. 10a). In other words, the emission spectra of the two different sets of fluorinated compounds have opposite shapes. Unlike absorption in solution, the identity of the terminal functional group had virtually no effect on recorded solution emission maxima or its emissive range and only affected the intensities of the emission events (Fig. S3, S5 and S7).

Absorption in the crystalline state extended up to 450–475 nm for most five ring structures, which is reflected in their yellow colouring as a powder and thin film (Fig. S2, S4, S6 and S8). However, some samples, like **BF2-Cl** and **TF$_2$T-F**, show an onset of absorption that almost reaches 600 nm. These differences in solid state absorption do not exclusively depend on changes in molecular properties, but are also caused by differences in crystal structures, alignment in the films, and film thickness. One trend worth mentioning is the hypsochromic shift of approximately 20–25 nm for the longest wavelength absorption maxima relative to their solution maxima, except for **FFBo-Cl**, which had similar maxima in the solid-state as in solution.

Emission in the crystalline state displayed the greatest variation between compounds, however, one trend that appears consistent across most fluorinated structures is that chlorine as the terminal functional group demonstrated greater fluorescence intensity than when fluorine was used (Fig. 10b and 12). **TF$_2$TF$_3$** and **TF$_2$T-Cl** have similar emission spectra, while **TF$_2$T-F** gives a significantly different spectrum for no obvious reasons (Fig. 10b). Additionally, **TF$_2$T-F** emitted up to 730 nm, which is 65 nm more than **TF$_2$TF$_3$** and **TF$_2$T-Cl**. As in solution, the emission of the shorter **TF$_3$** is blue shifted by 20–30 nm and about 70 nm in the crystalline state relative to **TTF$_3$** (Fig. 10b). Emission spectra for compounds where either the benzene or the benzoxazole ring are fluorinated have rather similar shapes, all with a shoulder towards longer wavelengths (Fig. 12).

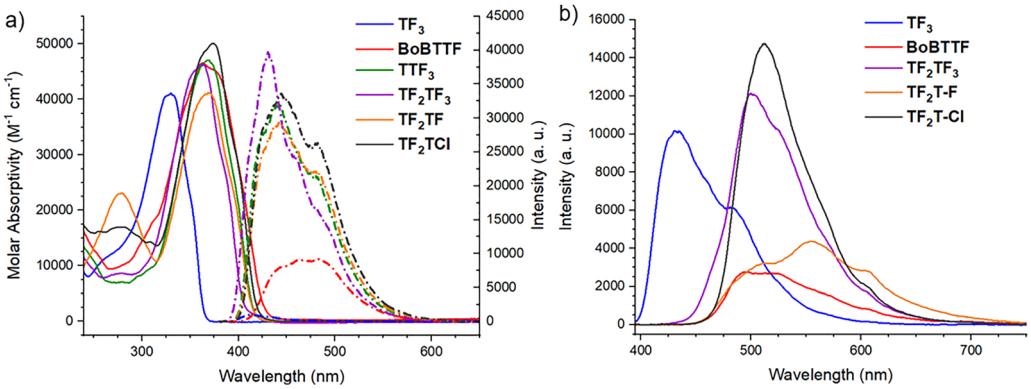

Fig. 10 Absorption and emission spectra of derivatives with the bithiophene moiety partially or fully fluorinated in (a) CH_2Cl_2 and (b) as thin films sandwiched between quartz slides. λ_{Exc} = 365 nm for both.

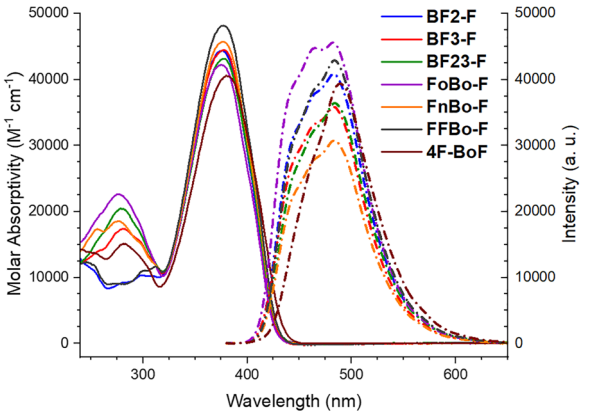

Fig. 11 Absorption and emission spectra of core-only calamitics with the inner benzene ring or benzoxazole's benzene ring partially or fully fluorinated in CH_2Cl_2. (λ_{Exc} = 365 nm).

These spectra matched more closely to those for TF_2TF_3 and TF_2T-Cl. Emission for the compounds **BF23-X** is an outlier relative to other fluorinated **BoBTTX** compounds in two ways: (i) higher emissive intensity was observed when fluorine is the terminal X group instead of chlorine and (ii) the start of the emission event for **BF23-Cl** was bathochromically shifted by 20 nm relative to **BF23-F**, yet emission ended at similar wavelengths (Fig. 12a). Emission spectra of **4FBo-Cl** behaved similarly to **FFBo-Cl** in that only one main emission maximum (525 nm with a small shoulder at 605 nm) was observed, while **4FBo-F** had significantly reduced emission intensity which produces a smaller emission range.

Variable temperature emission for **BF2-F** as a thin film was performed to assess the extent of fluorescence that persists as the sample melts through different mesophases of reduced order (*i.e.* greater mobility) up and into the isotropic liquid. Fluorescence intensity is shown to decrease as melting into progressively more fluid-like (meso)phases occurs (Fig. 13), which coincides naturally with increasing temperature, and this is a predictable result given that increasing molecular motion and vibrational coupling would permit for greater radiationless relaxation.[54] Also noteworthy is the hypsochromic shift that occurs as the phase becomes less ordered, which is most significant for the crystal to SmA phase transition (by ≈70 nm), while only minor shifts occur between remaining transitions of these fluid (meso)phases (by 6 nm from SmA to N, and 15 nm from N to Iso) (Fig. 12). These results coincide with previously reported temperature-dependent, solid-state emission studies on calamitic LCs where such changes in

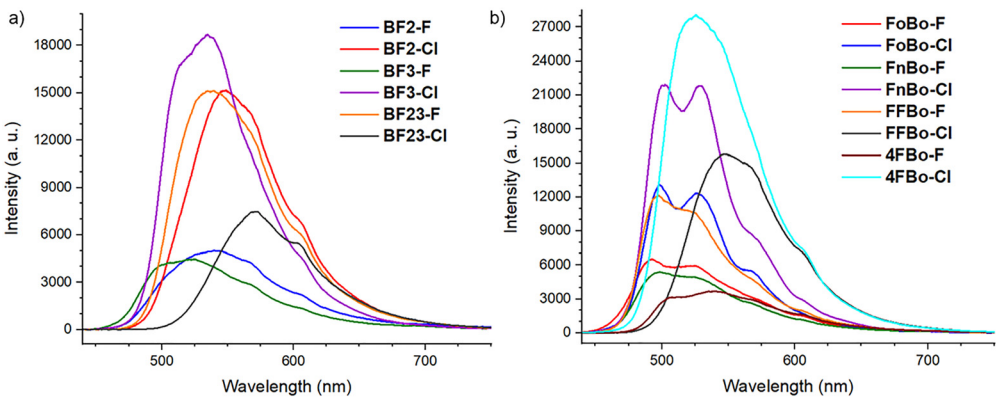

Fig. 12 Emission spectra of core-only calamitics as a thin film between quartz slides where (a) the inner benzene ring is partially fluorinated; or (b) benzoxazole's benzene ring is partially or fully fluorinated. (λ_{Exc} = 365 nm for both sets of spectra and the sample temperature was 23 °C (crystalline phases)).

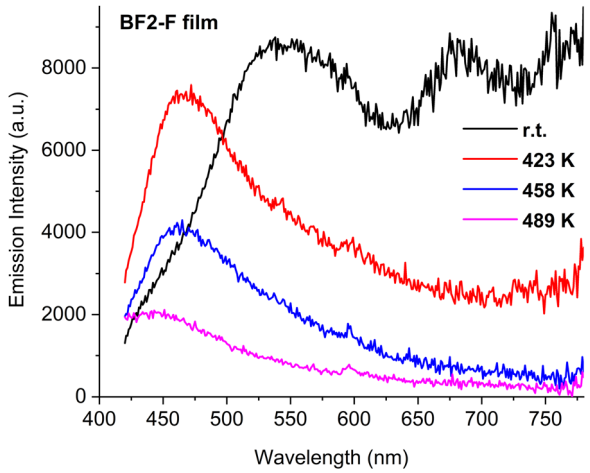

Fig. 13 Variable temperature emission spectra of **BF2-F** as a thin film sandwiched between quartz slides in the crystalline phase (black line, r. t. = 22–24 °C (295–297 K)), liquid crystalline SmA phase (red line, 150 °C (423 K)), liquid crystalline N phase (blue line, 185 °C (459 K)), and isotropic liquid phase (pink line, 216 °C (489 K)). (λ_{Exc} = 400 nm).

fluorescence intensity between the different (meso)phases was proposed to be useful within sensing applications.[55]

Conclusion

Synthetic approaches for the sequential lateral fluorination of our recently developed template for core-only calamitic liquid crystals **BoBTTX** (benzoxazole-benzene-thiophene-thiophene) were developed successfully. The presence of fluorine substituents on conjugated building blocks benzoxazole, benzene, and thiophenes was tolerated in all reactions performed herein, although general trends of decreased reactivity were observed due to fluorine's inductive electron withdrawing capabilities, especially when multiple of them were attached to these aromatic rings. All fluorinated **BoBTTX** derivatives display mesomorphism, yet systematic fluorination of each conjugated ring gave extremely varied liquid crystal behaviour. Most successful results (*i.e.* lower phase transition temperatures, wider liquid crystal windows) were obtained when fluorine substituents are attached to the central benzene unit. Incorporation of only one fluorine substituent achieved reductions to the melting/crystallization temperatures by 60 °C, giving mesomorphic character down to temperatures around 130 °C. This is a remarkable feat for a calamitic liquid crystal composed of five aromatic rings without side-chains. These results demonstrate how core-only calamitics can achieve comparable mesophase temperatures to similar side-chain bearing calamitic structures and enables their application as organic semiconductor in conventional devices. Clearly, lateral fluorination is an excellent method for producing a wide variety of mesomorphic properties within a singular mesogenic core, especially one with no side-chains. Study of the optoelectronic properties of the fluorinated **BoBTTX** derivatives demonstrated strong absorption and emission peaks between 340–400 nm and 500–580 nm, respectively, in solution and the crystal phase. It is also shown that these compounds are fluorescent in their liquid crystal and isotropic liquid phases, although their emission peak decreases and is blue-shifted with increasing temperature.

Conflicts of interest

There are no conflicts to declare.

Data availability

All data are available as supplementary information (SI). Supplementary information: detailed synthetic procedures and spectroscopic data, thermal analysis data (polarized optical microscopy, DSC, pXRD), single crystal data, and details of DFT calculations. See DOI: **https://doi.org/10.1039/d5tc02621k**.

CCDC 2393984 contains the supplementary crystallographic data for this paper.[56]

Acknowledgements

SHE (RGPIN-2019-07271) and JGR (CGSM/CGSD) acknowledge financial support from the Natural Sciences and Engineering Research Council of Canada. SHE also thanks the Canadian Foundation for Innovation and the Ontario Innovation Trust for funding (JELF 36776). WGS thanks the Natural Sciences and Engineering Council Canada (NSERC) and Canada Foundation for the Innovation for Discovery and infrastructure grants, respectively. WGS additionally acknowledges the Quebec Center for Advanced Materials (CQMF) and the Institut Courtois for access to additional equipment. D. Chartrand is also thanked for technical assistance with the low temperature equipment.

References

1 J. W. Goodby, R. E. Mandle, E. J. Davis, T. Zhong and S. J. Cowling, *Liq. Cryst.*, 2015, **42**, 593–622.
2 T. J. Dingemans, N. S. Murthy and E. T. Samulski, *J. Phys. Chem. B*, 2001, **105**, 8845–8860.
3 N. A. Zafiropoulos, E.-J. Choi, T. Dingemans, W. Lin and E. T. Samulski, *Chem. Mater.*, 2008, **20**, 3821–3831.
4 S. Kuiper, W. F. Jager, T. J. Dingemans and S. J. Picken, *Liq. Cryst.*, 2009, **36**, 389–396.
5 S. K. J. Lim, R. Rahamathullah, N. M. Sarih and W. M. Khairul, *J. Lumin.*, 2018, **201**, 397–401.
6 R. J. Twieg, V. Chu, C. Nguyen, C. M. Dannels and C. Viney, *Liq. Cryst.*, 1996, **20**, 287–292.
7 J. G. Rothera, J. Yu, K. AlNajm, R. Butrus, E. Ahangari-Bashash, L. K. Watanabe, J. M. Rawson, A. Dmitrienko, V. N. Vukotic and S. H. Eichhorn, *Chem. – Asian J.*, 2025, **20**, e202401543.
8 M. Funahashi, *Polym. J.*, 2017, **49**, 75–83.
9 H. Iino and J. Hanna, *Polym. J.*, 2017, **49**, 23–30.
10 H. Iino, T. Usui and J. Hanna, *Nat. Commun.*, 2015, **6**, 6828.

11 M. J. Han, D. Wei, Y. H. Kim, H. Ahn, T. J. Shin, N. A. Clark, D. M. Walba and D. K. Yoon, *ACS Cent. Sci.*, 2018, **4**, 1495–1502.
12 C. Tschierske, in *Liquid Crystals*, ed. C. Tschierske, Springer Berlin Heidelberg, Berlin, Heidelberg, 2011, vol. 318, pp. 1–108.
13 M. Hird, *Chem. Soc. Rev.*, 2007, **36**, 2070.
14 M. Hird, J. W. Goodby, R. A. Lewis and K. J. Toyne, *Mol. Cryst. Liq. Cryst.*, 2003, **401**, 1–18.
15 M. Hird and K. J. Toyne, *Mol. Cryst. Liq. Cryst.*, 1998, **323**, 1–67.
16 K. D. Katariya, K. J. Nakum and M. Hagar, *Liq. Cryst.*, 2022, **49**, 312–326.
17 A. S. Radwan and M. M. Makhlouf, *J. Lumin.*, 2021, **36**, 1751–1760.
18 Y. Song, J. Li, R. Xia, H. Xu, X. Zhang, H. Lei, W. Peng, S. Dai, S. Aya and M. Huang, *Phys. Chem. Chem. Phys.*, 2022, **24**, 11536–11543.
19 M. J. Shirodkar, K. S. Bhat, D. Bhattacharjee, M. K. Sonali, M. G. Mahesha and P. Bhagavath, *Sci. Rep.*, 2025, **15**, 15540.
20 Y. Qian, S. Li, H. Tang, J. Sun, M. Cai, T. Zhao, C. Yang, W. Ye and Z. Zhang, *J. Mol. Liq.*, 2023, **391**, 123289.
21 P. Kirsch, *J. Fluor. Chem.*, 2015, **177**, 29–36.
22 P. Kirsch, W. Binder, A. Hahn, K. Jährling, M. Lenges, L. Lietzau, D. Maillard, V. Meyer, E. Poetsch, A. Ruhl, G. Unger and R. Fröhlich, *Eur. J. Org. Chem.*, 2008, 3479–3487.
23 G. W. Gray, D. Lacey, J. E. Stanton and K. J. Toyne, *Liq. Cryst.*, 1986, **1**, 407–413.
24 H.-W. Keum, S.-D. Roh, Y. S. Do, J.-H. Lee and Y.-B. Kim, *Mol. Cryst. Liq. Cryst.*, 2005, **439**, 189/[2055]–199/[2065].
25 P. J. Collings and M. Hird, *Introduction to Liquid Crystals Chemistry and Physics*, CRC Press, 1st edn, 2017.
26 Q. Guo, K. Yan, V. Chigrinov, H. Zhao and M. Tribelsky, *Crystals*, 2019, **9**, 470.
27 J. Li, X. Yang, N. Gan, B. Wu and Z. An, *Liq. Cryst.*, 2015, **42**, 397–403.
28 M. Pytlarczyk, E. Dmochowska, M. Czerwiński and J. Herman, *J. Mol. Liq.*, 2019, **292**, 111379.
29 B. Li, W. He, L. Wang, X. Xiao and H. Yang, *Soft Matter*, 2013, **9**, 1172–1177.
30 G. W. Gray, M. Hird, D. Lacey and K. J. Toyne, *Mol. Cryst. Liq. Cryst.*, 1989, **172**, 165–189.
31 A. S. Matharu, S. J. Cowling and G. Wright, *Liq. Cryst.*, 2007, **34**, 489–506.
32 K. Hu, Y. Xu, P. Chen, A. Gao, W. Du, X. Chen and Z. An, *Liq. Cryst.*, 2014, **41**, 1455–1464.
33 J. Li, L. Mo, Z. Che, J. Li, M. Hu, D. Wan and Z. An, *Liq. Cryst.*, 2022, **49**, 1753–1762.
34 M. Hird, K. J. Toyne, G. W. Gray, D. G. McDonnell and I. C. Sage, *Liq. Cryst.*, 1995, **18**, 1–11.
35 G. W. Gray, M. Hird and K. J. Toyne, *Mol. Cryst. Liq. Cryst.*, 1991, **195**, 221–237.
36 P. Dasgupta, A. Pramanik, M. K. Das and B. Das, *Liq. Cryst.*, 2015, **42**, 1083–1094.
37 Y. Sakamoto, S. Komatsu and T. Suzuki, *J. Am. Chem. Soc.*, 2001, **123**, 4643–4644.
38 R. D. Viirre, G. Evindar and R. A. Batey, *J. Org. Chem.*, 2008, **73**, 3452–3459.
39 P. Espinet and A. M. Echavarren, *Angew. Chem., Int. Ed.*, 2004, **43**, 4704–4734.
40 S. E. Denmark, R. C. Smith and W.-T. T. Chang, *Tetrahedron*, 2011, **67**, 4391–4396.
41 F. Witte, S. P. Zucker, B. Paulus and C. C. Tzschucke, *Organometallics*, 2021, **40**, 591–599.
42 S. Llona-Minguez, A. Höglund, A. Ghassemian, M. Desroses, J. M. Calderón-Montaño, E. Burgos Morón, N. C. K. Valerie, E. Wiita, I. Almlöf, T. Koolmeister, A. Mateus, C. Cazares-Körner, K. Sanjiv, E. Homan, O. Loseva, P. Baranczewski, M. Darabi, A. Mehdizadeh, S. Fayezi, A.-S. Jemth, U. Warpman Berglund, K. Sigmundsson, T. Lundbäck, A. Jenmalm Jensen, P. Artursson, M. Scobie and T. Helleday, *J. Med. Chem.*, 2017, **60**, 4279–4292.
43 Z.-Z. Huang, X.-M. Yan and X.-R. Mao, *Heterocycles*, 2011, **83**, 1371.
44 R. Wang, H. Lu, M. Yan, M. Li, X. Lv, H. Huang, A. Ghaderi, T. Iwasaki, N. Kambe, A. Abdukader and R. Qiu, *J. Mater. Chem. C*, 2021, **9**, 12545–12549.
45 K. Hu, P. Chen, Q. Weng, D. Shi, R. Chen, X. Chen and Z. An, *Liq. Cryst.*, 2015, 1–11.
46 Y. Xu, X. Chen, F. Zhao, X. Fan, P. Chen and Z. An, *Liq. Cryst.*, 2013, **40**, 197–215.
47 G. Wright, *PhD Dissertation*, Nottingham Trent University, 1996.
48 G. W. Gray, M. Hird, D. Lacey and K. J. Toyne, *J. Chem. Soc. Perkin Trans.*, 1989, 2041–2053.
49 W. Maier and A. Saupe, *Z. Naturforsch., A:Phys. Sci.*, 1959, **14**, 882–889.
50 T. Nozawa, P. E. Brumby and K. Yasuoka, *Int. J. Mol. Sci.*, 2018, **19**, 2715.
51 R. J. C. Brown and R. F. C. Brown, *J. Chem. Educ.*, 2000, **77**, 724.
52 C. J. Pace and J. Gao, *Acc. Chem. Res.*, 2013, **46**, 907–915.
53 V. Percec, G. Johansson, G. Ungar and J. Zhou, *J. Am. Chem. Soc.*, 1996, **118**, 9855–9866.
54 H. Mauser and G. Gauglitz, in *Comprehensive Chemical Kinetics*, Elsevier, 1998, vol. 36, pp. 241–297.
55 S. A. Oladepo, *J. Mol. Liq.*, 2021, **323**, 114590.
56 CCDC 2393984: Experimental Crystal Structure Determination, 2025, DOI: **10.5517/ccdc.csd.cc2lc49f**.